Ceramics-Silikáty 64 (2), 172-179 (2020)
www.ceramics-silikaty.cz doi: 10.13168/cs.2020.0006

EFFECT OF Ni DOPING AND SYNTHESIS TEMPERATURE ON THE PROPERTIES OF NIR-REFLECTIVE $ZnFe_2O_4$ BLACK PIGMENTS

#MANTANA SUWAN, NUCHJARIN SANGWONG, SITTHISUNTORN SUPOTHINA

National Metal and Materials Technology Center, National Science and Technology Development Agency (NSTDA), 114 Thailand Science Park Phahonyothin Rd., Khlong Luang, Pathum Thani 12120, Thailand

#E-mail: mantanas@mtec.or.th

Submitted September 26, 2019, accepted November 6, 2019

Keywords: Zinc Ferrite, NIR-Reflective Pigment, Cool Pigment, Black Pigment, Solid-State Reaction

NIR-reflective Ni-doped $ZnFe_2O_4$ black pigments with the general formula of $Zn_{(1-x)}Ni_xFe_2O_4$ have been synthesized by a conventional solid-state reaction of ZnO, Fe_2O_3 and NiO. The effect of Ni doping was studied by adding various amounts of NiO, with x ranging from 0 to 1. Proportional amounts of ZnO, Fe_2O_3 and NiO were homogeneously mixed together by means of wet milling, followed by filtration and drying. Then, the mixtures were calcined at 1000 and 1100 °C for 3 h. XRD analysis of the undoped pigments revealed the presence of pure $ZnFe_2O_4$ in all synthesis conditions. The addition of NiO dopant into the $ZnFe_2O_4$ caused a gradual shift of the diffraction peaks toward higher angles due to the substitution of Zn^{2+} by the smaller Ni^{2+} to form the $Zn_{(1-x)}Ni_xFe_2O_4$. Upon the increase of NiO doping content and calcination temperature, the color hue of the pigments changed from light brown to brownish black, and a gradual reduction of the NIR reflectance was observed. For the black pigments which were synthesized at 1100 °C, the band-gap energy changed from 2.05 eV for $ZnFe_2O_4$ (x = 0) to 1.65 eV for $NiFe_2O_4$ (x = 1). At the optimum synthesis condition, resulting in black color hue and high NIR reflectance, the $Zn_{0.5}Ni_{0.5}Fe_2O_4$ pigment synthesized at 1100 °C had high NIR reflectance of 55.3 %.

INTRODUCTION

Solar radiation, which comprises of approximately 5 % ultraviolet (UV), 43 % visible and 52 % near-infrared (NIR), can be largely absorbed by buildings and concrete constructions. An increase of the heat produced in the building envelop can transfer further into the building, resulting in large energy consumption of cooling systems, especially in summer. Therefore, NIR-reflective coatings for the building envelop have been proposed as an efficient and sustainable alternative to reduce this heat production. It has been reported that the use of NIR-reflective materials can significantly improve building comfort and reduce the energy consumption of air-conditioning units [1-3]. In particular, if the exterior surface of roofs and walls is covered by NIR-reflective coatings, the heat accumulated in the building is significantly reduced.

Generally, white pigments such as TiO_2 and SiO_2 are well known for their high solar reflectivity. However, white pigments are not commonly used for exterior coating of building envelops due to aesthetic reasons and the ease of being contaminated in urban environments. For this reason, non-white pigments with high NIR reflectance are more attractive. This topic has gained more attention over the past decades. So far, various types of NIR-reflective pigments exhibiting blue [4-6], green [7-9], yellow [10-14] and brown [10-12, 15-16] color hues were synthesized by several methods, including co-precipitation, hydrothermal, sol-gel, solid-state reaction, etc. Recently, special interest has been paid to the preparation of NIR-reflective dark pigments for roof coating. For instance, Liu et al. synthesized Mg-doped $ZnFe_2O_4$ pigments with a color hue ranging from brick red to brownish black. The pigments exhibited NIR reflectance ranging from 51 to 58 % depending on the Mg doping content [16]. Sanada et al. synthesized Co- and Al-doped $CoFe_2O_4$ pigments of various colors ranging from greenish black, brownish black and black [17]. The reflectance of these pigments is in a range of 18.0 to 51.4 % in the visible-NIR regions, with the reflectance of the most blackish pigment being 18.0 %. Oka and Masui synthesized high NIR-reflective $Ca_2Mn_{1-x}Ti_xO_4$ black pigments with reflectance ranging from 50.1 to 72.5 in the NIR region [18]. At the optimum composition x = 0.15, the $Ca_2Mn_{0.85}Ti_{0.15}O_4$ pigment exhibited NIR reflectance of 66.2 %. Bao et al. investigated the effect of doping ferric ion (Fe^{3+}) for Al^{3+} ion of the $Co_{0.5}Mg_{0.5}Al_2O_4$ blue pigment [19]. A series of $Co_{0.5}Mg_{0.5}Al_{2-x}Fe_xO_4$ pigments with color hue ranging from blue to blackish blue to black and NIR reflectance in a range of 45.7-54.2 % were obtained. Pigments with darker color hue and decreased NIR reflectance were obtained by doping with the Fe^{3+}.

In the present study, Ni-doped $ZnFe_2O_4$ reflective black pigment ($Zn_{(1-x)}Ni_xFe_2O_4$, x = 0, 0.1, 0.3, 0.5, 0.75 and 1.0) was synthesized. Effects of calcination temperature and Ni doping content on the properties of the pigments were investigated. An optimum synthesis condition that yields pigments having dark color hue and high NIR-reflectance was suggested. The solid-state

synthesis was selected owing to its process simplicity and feasibility for large-scale production. In addition, the main process and required equipment are common in the ceramic industry.

EXPERIMENTAL

Synthesis of Ni-doped $ZnFe_2O_4$ pigments

Undoped $ZnFe_2O_4$ was obtained by calcination of raw materials comprising stoichiomtric amounts of ZnO (Cernic International Co., Ltd.) and Fe_2O_3 (NIC Interchem Co.Ltd.). Various amounts of NiO (Sigma Aldrich) dopant were added into the starting raw materials in the range of x = 0 to 1 to study the effect of Ni doping. The mixture was mixed by wet ball milling in acetone, and then subjected to calcination at temperatures of 1000 and 1100 °C for 3 h. The obtained pigments were grounded in a mortar, washed 3 times with de-ionized water and dried at 105 °C for at least 5 h. After grinding into fine powder by ball milling, the pigments were sieved through a 325-mesh screen.

Characterization

A Rigaku TTRAX III X-ray diffractometer was employed for crystalline phase identification. A Cary 5000 UV-Vis-NIR spectrophotometer, equipped with an integrating sphere, was employed for acquiring diffuse reflectance spectra. The NIR reflectance (R) was derived from the reflectance in a wavelength range of 700 - 2500 nm following the ASTM E903-96 standard. The R was determined via the relation

$$R = \frac{\int_{700}^{2500} r(\lambda)\, i(\lambda)\, d(\lambda)}{\int_{700}^{2500} i(\lambda)\, d(\lambda)} \quad , \qquad (1)$$

where $r(\lambda)$ is the reflectance ($W \cdot m^{-2}$), and $i(\lambda)$ is the solar irradiance ($W \cdot m^{-2} \cdot nm^{-1}$) obtained from the ASTM E903-96 standard.

The optical band-gap energy (E_g) was determined according to the Kubelka-Munk function which is given by [20]

$$\alpha = F(R) = \frac{(1-R)^2}{2R} \quad , \qquad (2)$$

where $F(R)$ is the Kubelka-Munk function, α is the absorption coefficient and R is the reflectance. The relationship between the absorption coefficient and the band gap is

$$\alpha\, h\, v = A(hv - E_g)^n, \qquad (3)$$

where α is the absorption coefficient, h is Plank's constant, v is the light frequency and A is a proportional constant. The power n is taken as ½ for a direct transition and 2 for an indirect transition. The E_g was determined by extrapolating of linear region on a plot of $(F(R)hv)^2$ vs. hv to $(F(R)hv)^2 = 0$.

The color hue was determined by the CIE $L^*a^*b^*$ colorimetric method using a spectrophotometer (Konica Minolta, CM-2600d). The L^* axis represents the lightness. The (+) a^* axis represents the red, while the (–) a^* represents the green. The (+) b^* axis represents the yellow, while the (–) b^* axis represents the blue. Particle morphology was observed with a Hitachi SU5000 field-emission scanning electron microscope (FE-SEM). An average particle size was determined from SEM images using image processing software (ImageJ).

RESULTS AND DISCUSSION

Figure 1 shows XRD patterns of the raw material and the products after calcination at 1000 and 1100 °C. It is evident that the XRD patterns of both pigments are practically identical. They are well defined and consist of strong reflection peaks at diffraction angles (2θ) of 29.9, 35.3, 36.9, 42.8, 53.1, 56.6, 62.2, 70.5, 73.5, 74.5 and 78.4 degrees which are attributed to (220), (311), (222), (400), (422), (511), (440), (620), (533), (622) and (444) planes, respectively. The diffraction patterns are in good agreement with the standard pattern of a spinel $ZnFe_2O_4$ (ICDD no. 00-022-1012). The well-defined XRD patterns without any other phases of the ZnO and Fe_2O_3 raw material indicate a completed solid-state reaction. Calcination at higher temperature (1100 °C) resulted in a sharper and more intense pattern, indicating an increase of crystallinity.

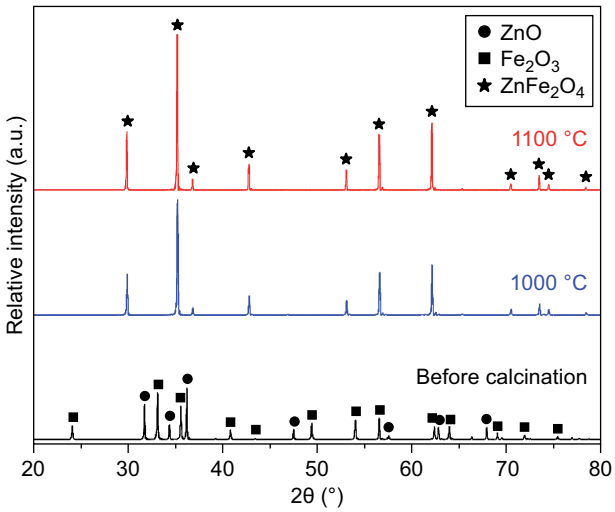

Figure 1. X-ray diffraction patterns of the raw material and the synthesized pigments.

Figure 2 shows XRD patterns of Ni-doped pigments synthesized at 1000 and 1100 °C. In general, XRD patterns of the Ni-doped $ZnFe_2O_4$ are similar to the

patterns of the undoped $ZnFe_2O_4$, indicating no change of the crystal structure. However, the XRD patterns of the Ni-doped $ZnFe_2O_4$ show a gradual shift of the reflection peaks toward higher 2θ angle. This peak shift can be explained by the substitution of a smaller Ni^{2+} for a larger Zn^{2+} (ionic radius of Ni^{2+} and Zn^{2+} = 0.55 and 0.60 Å, respectively [21]). The extent of shifting increases with an increased amount of Ni doping. At x = 1, the XRD pattern can be well matched with the standard pattern of the $NiFe_2O_4$ (ICDD no. 01-081-8428), confirming complete substitution of Zn^{2+} by Ni^{2+}. This observation is in good agreement with a shift of XRD peaks toward higher 2θ due to the substitution of smaller Mg^{2+} for Zn^{2+} in the Mg-doped $ZnFe_2O_4$ [16]. Note that the Ni-doped pigment synthesized at 1000°C comprised of minor phase of unreacted Fe_2O_3 raw material at $x \geq 0.5$. However, it was disappeared at higher calcination temperature due to the completed solid-state reaction.

Figure 3 shows UV-Vis-NIR diffuse reflectance spectra of the $Zn_{(1-x)}Ni_xFe_2O_4$ pigments. All pigments show low reflectance in a wavelength range of around 300 to 650 nm, and characteristic absorption bands of $ZnFe_2O_4$ at around 700-800 and 1000-1400 nm, which are attributed to ${}^6A_{1g} \rightarrow {}^4T_{2g}$ and ${}^6A_{1g} \rightarrow {}^4T_{1g}$ for *d-d* electron transition of Fe^{3+} [22]. The reflectance increases at wavelengths higher than 1500 nm. NIR reflectance of the $ZnFe_2O_4$ pigments synthesized at 1000 and 1100 °C are 65.9 and 61.2 %, respectively. At 1000 °C, the addition of Ni has no significant effect on the diffuse reflectance spectrum. The NIR reflectance only slightly decreases from 65.9 % for the undoped $ZnFe_2O_4$ to 62.2 % for the $NiFe_2O_4$ (x = 1). However, a significant decrease in the reflectance spectrum, particularly at wavelengths higher than 1500 nm, was observed for the pigments synthesized at 1100 °C. The NIR reflectance significantly decreases from 61.2 % for the undoped $ZnFe_2O_4$ to 52.0 % for the $NiFe_2O_4$.

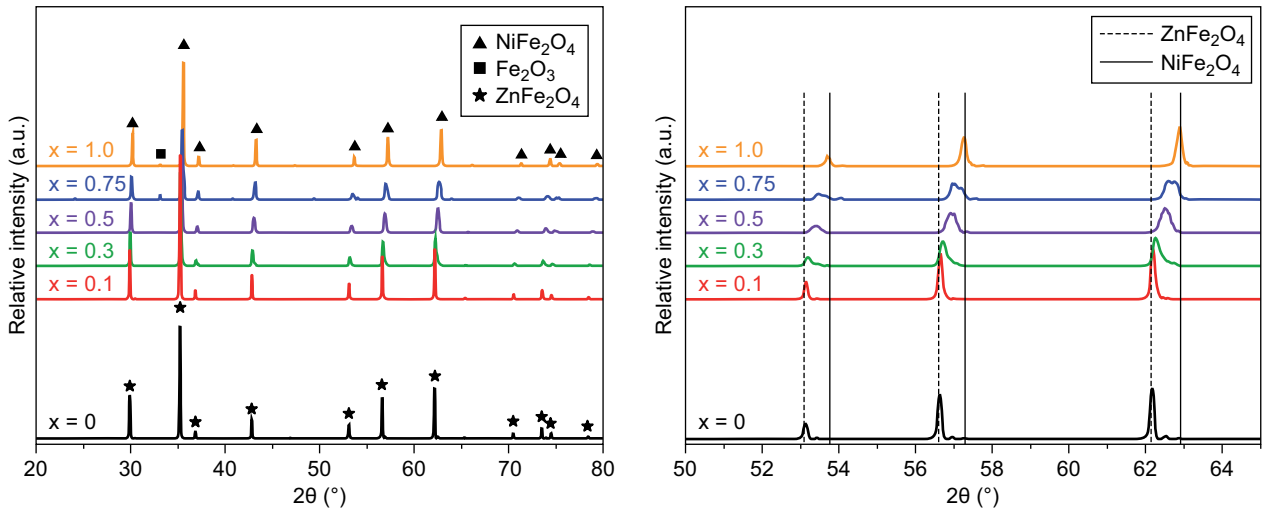

a) 1000 °C

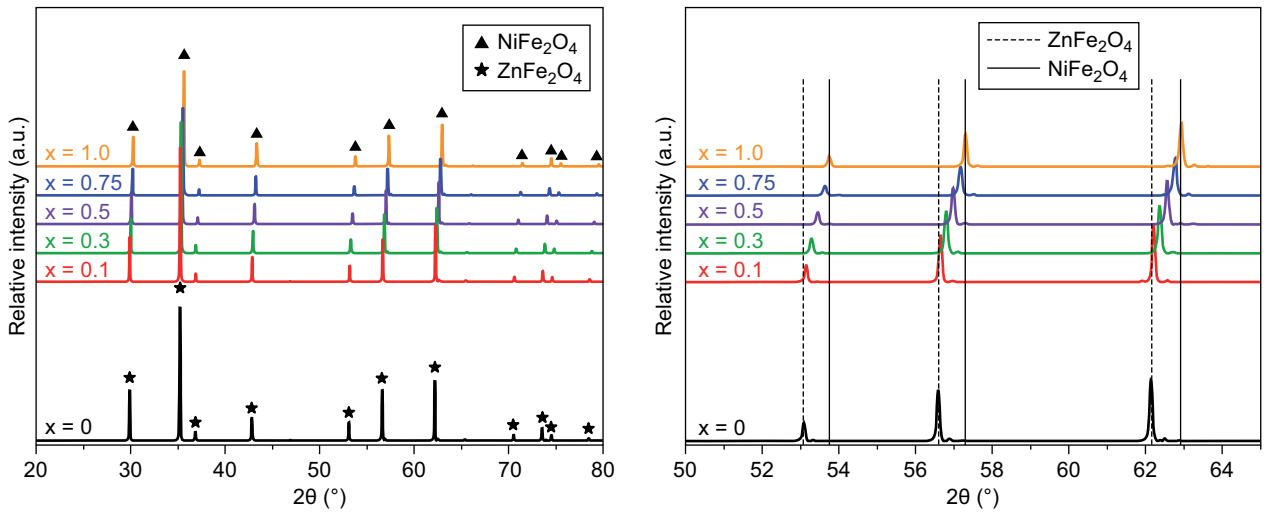

b) 1100 °C

Figure 2. X-ray diffraction patterns of the $Zn_{(1-x)}Ni_xFe_2O_4$ pigments synthesized at: a) 1000 °C and b) 1100 °C.

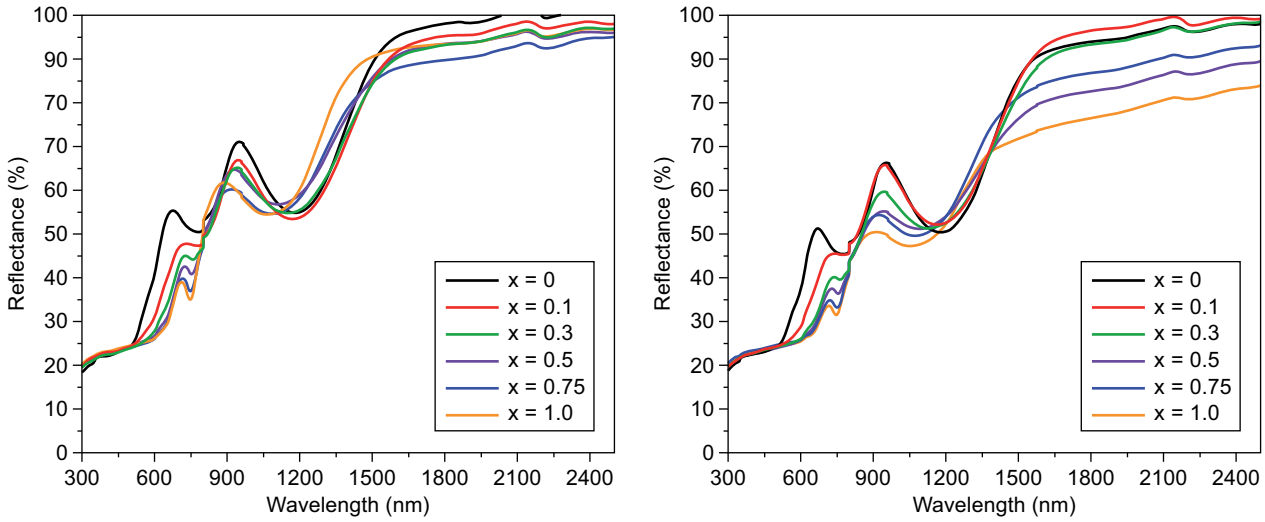

a) 1000 °C b) 1100 °C

Figure 3. Diffuse reflectance spectra of the $Zn_{(1-x)}Ni_xFe_2O_4$ pigments synthesized at: a) 1000 °C and b) 1100 °C.

It has been realized that a change of total reflectance can be attributed to a change of absorption in a certain wavebands as a result of alteration of atomic and electronic structure of a host lattice by doping atoms. For instance, doping $ZnFe_2O_4$ with Co results in a reduction of the characteristics absorption bands centered at around 770 and 1200 nm upon the increased amount of the Co dopant. In contrast, the incorporation of Pr has no effect on characteristics absorption bands of the $ZnFe_2O_4$ because larger Pr atom cannot substitute for the Co site [23]. Doping both tetrahedron and octahedron sites of the ferrite has been reported in $Co_{0.5}Mg_{0.5}Al_{2-x}Fe_xO_4$ pigment [19]. The pigments exhibit stronger absorption in the visible region and increasing NIR reflectance upon an increasing content of Fe^{3+}, resulting in a change of color hue from blue for x = 0 to dark for x = 1, and a decrease of NIR reflectance from 54.2 to 45.7 %. In the present work, the effect of Ni doping on the reflectance is more significant for the pigments synthesized at 1100 °C. A decrease of reflectance is observed in a wavelength ranges of around 500-800 nm and >1400 nm.

Figure 4 shows the color hues of pigments with various Ni doping content. $L^*a^*b^*$ color coordinates are summarized in Table 1. The color hue changes from light brown to brownish black with increasing Ni content and synthesis temperature. The values of lightness L^* significantly decrease from > 47 for the undoped pigments to around 28-29 for the pigments doped with Ni.

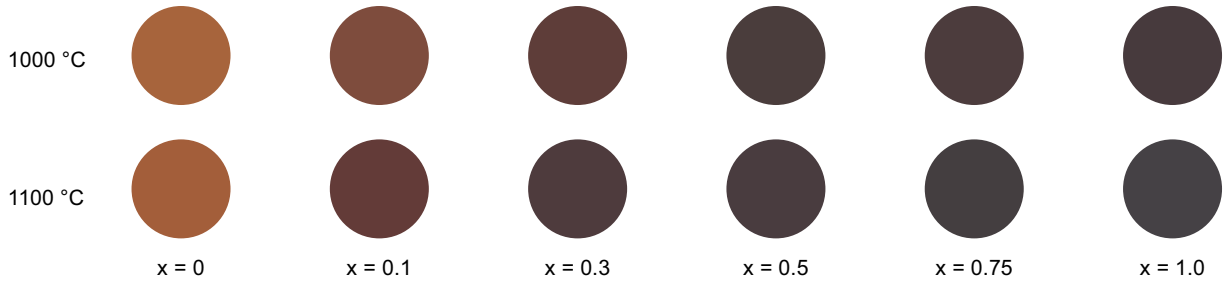

Figure 4. Color hues of the $Zn_{(1-x)}Ni_xFe_2O_4$ pigments.

Table 1. Color coordinates, NIR reflectance and band-gap energy of $Zn_{(1-x)}Ni_xFe_2O_4$ pigments.

x (mole)	1000 °C					1100 °C				
	L^*	a^*	b^*	R (%)	E_g (eV)	L^*	a^*	b^*	R (%)	E_g (eV)
0	49.64	25.34	35.52	65.9	2.10	47.93	27.17	37.54	61.2	2.05
0.1	39.52	21.41	20.55	62.7	1.90	31.75	18.43	12.18	61.5	1.85
0.3	31.30	16.00	11.44	61.9	1.80	28.43	10.66	4.41	58.1	1.70
0.5	29.92	11.11	6.00	62.5	1.70	27.67	7.82	2.42	55.3	1.65
0.75	28.35	9.38	3.62	60.3	1.70	28.04	4.96	0.27	55.6	1.65
1.0	28.92	7.29	2.03	62.2	1.70	28.70	3.31	-0.59	52.0	1.65

It has been generally accepted that the lightness L^* is ≤ 30 for blackish pigment. Therefore, black pigments can be synthesized at 1000 °C with a Ni doping content ≥ 0.5 and at 1100 °C with a Ni doping content ≥ 0.3. In addition, low values of a^* and b^* are observed for the pigments synthesized at 1100 °C, indicating that the pigments are more blackish. Based on these results, the optimum composition was x = 0.5, and the optimum synthesis temperature was 1100 °C. The $Zn_{0.5}Ni_{0.5}Fe_2O_4$ pigment possesses a NIR reflectance of 55.3 % and an L^* value of 27.67, indicating high darkness and NIR reflectance.

The optical band-gap energy (E_g) of the $Zn_{(1-x)}Ni_xFe_2O_4$ pigments was derived from the diffuse reflectance spectra using the Kubelka-Munk method. Figure 5 shows a Tauc plot of $(F(R)h\upsilon)^2$ vs. E_g for the pigments

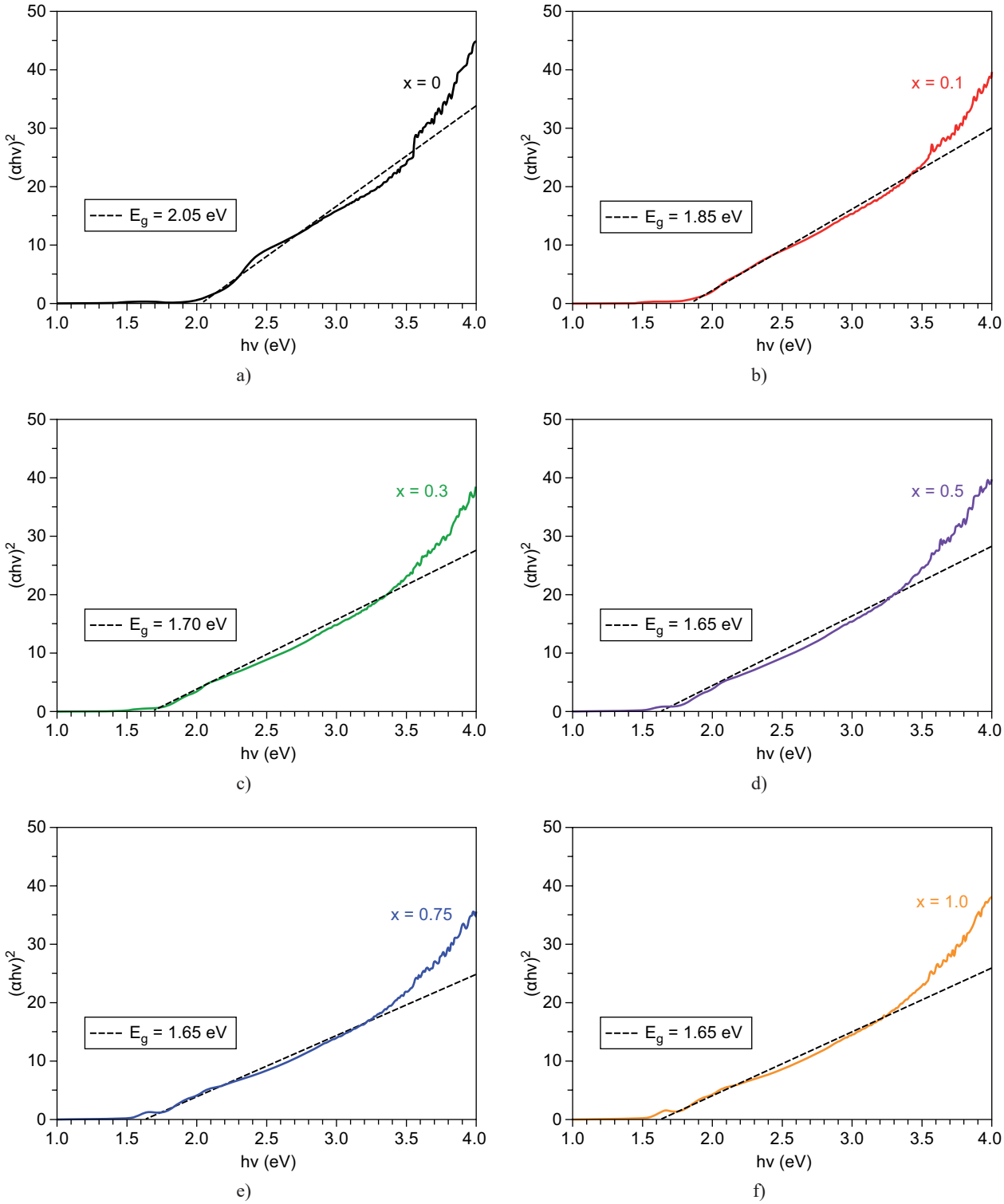

Figure 5. Kubelka-Munk transformed reflectance spectra of the $Zn_{(1-x)}Ni_xFe_2O_4$ pigments synthesized at 1100 °C.

synthesized at 1100 °C. The plots show linear regression when the exponent n is taken as 2, indicating indirect allowed transitions. Values of E_g for all synthesized pigments are summarized in Table 1. The E_g of $ZnFe_2O_4$ pigments synthesized at 1000 and 1100 °C are 2.10 and 2.05 eV, respectively, which is consistent with values reported in the literature [16, 24]. For the pigments synthesized at 1000 °C, the E_g gradually decreases from 2.10 eV to 1.70 eV (at x = 1) which corresponds to the band gap of $NiFe_2O_4$ [25]. A similar trend was observed for the pigments synthesized at 1100 °C. The band gap shift could be attributed to the replacement of Ni^{2+} for Zn^{2+} in $ZnFe_2O_4$ structure as described in the XRD analysis. A decrease of E_g upon an increased content of a dopant was observed in Mg-doped $ZnFe_2O_4$ [26] and Co-doped $ZnFe_2O_4$ [27-28]. It has been described that the value of E_g can be affected by various factors, such as crystallite size, structural parameter, and the presence of impurities [28-29]. In the present work, the Ni doping had no effect on the crystallite size of the pigments as summarized in Table 2. The decrease of E_g might be ascribed to the presence of additional sub-band-gap energy levels induced by the abundant surface and interface defects in the agglomerated nanoparticles [28, 30].

Table 2. An average particle size of the $Zn_{(1-x)}Ni_xFe_2O_4$ pigments.

x (mole)	Particle size (μm)	
	1000 °C	1100 °C
0	0.50 ± 0.11	0.83 ± 0.10
0.1	0.45 ± 0.08	0.71 ± 0.13
0.3	0.56 ± 0.14	0.78 ± 0.16
0.5	0.52 ± 0.10	0.71 ± 0.14
0.75	0.60 ± 0.14	0.81 ± 0.23
1.0	0.51 ± 0.10	0.79 ± 0.18

Figure 6 shows SEM images of the $Zn_{(1-x)}Ni_xFe_2O_4$ pigments. The average particle size determined from the SEM images using image processing software (ImageJ) is summarized in Table 2. In general, the particle morphology of the undoped and Ni-doped pigments is very similar. The undoped pigment synthesized at 1000 °C has an average particle size of 0.50 ± 0.11 μm, and the particles grew to 0.83 ± 0.10 μm after calcination at 1100 °C. Note that no significant change of the average particle size was observed upon the increase of NiO doping content.

CONCLUSIONS

Highly NIR-reflective $Zn_{(1-x)}Ni_xFe_2O_4$ black pigments were synthesized by a conventional solid-state reaction of ZnO, Fe_2O_3 and NiO at 1000 and 1100 C. The undoped $ZnFe_2O_4$ pigment had light brown color hue and exhibited NIR reflectances of 65.9 and 61.2 % at synthesis temperatures of 1000 and 1100 °C, respectively. The substitution of Zn^{2+} with Ni^{2+} resulted in a gradual decrease of the NIR reflectances to 62.2 and 52.0 % for the $NiFe_2O_4$ (x = 1.0) synthesized at 1000 and 1100 °C, respectively. It also resulted in a decrease in band-gap energy from ~ 2.1 eV for $ZnFe_2O_4$ to ~ 1.7 eV for $NiFe_2O_4$, and a color change from light brown to dark brown and brownish black upon the increase of Ni doping content. At the optimum synthesis condition, *i.e.* 1100 °C and x = 0.5, the $Zn_{0.5}Ni_{0.5}Fe_2O_4$ pigment had black color hue with $L^* = 27.67$, $a^* = 7.82$ and $b^* = 2.42$, and a high NIR reflectance of 55.3 %.

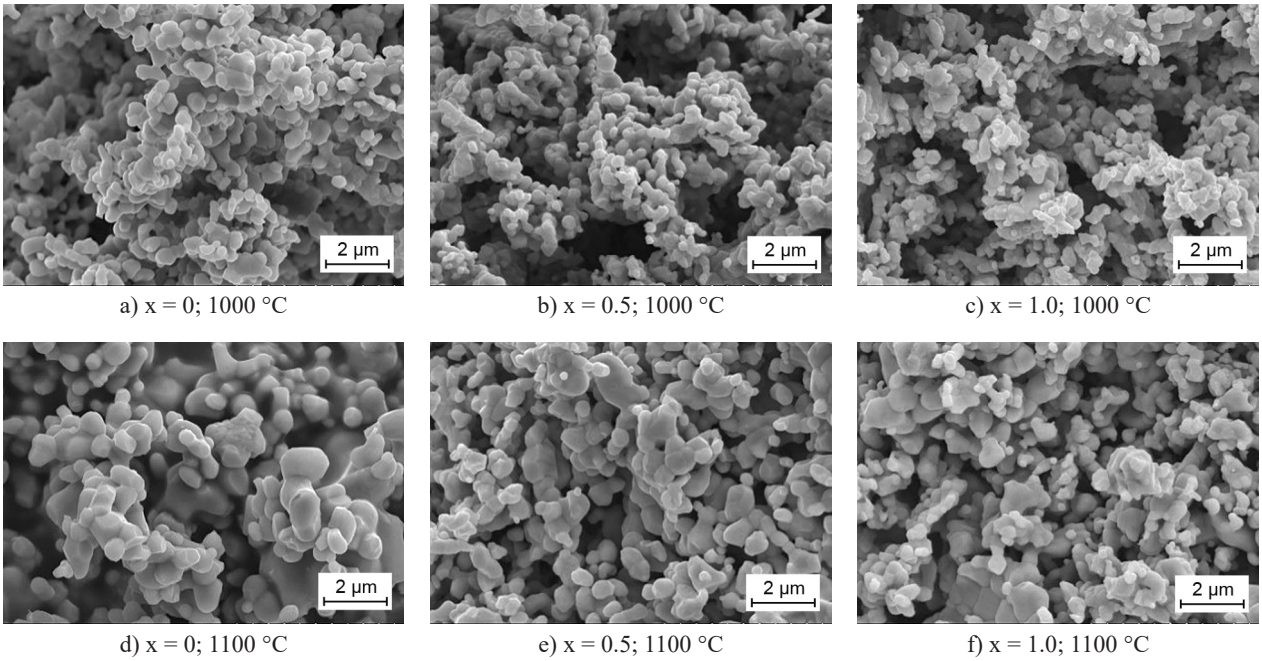

a) x = 0; 1000 °C b) x = 0.5; 1000 °C c) x = 1.0; 1000 °C

d) x = 0; 1100 °C e) x = 0.5; 1100 °C f) x = 1.0; 1100 °C

Figure 6. SEM images of the $Zn_{(1-x)}Ni_xFe_2O_4$ pigments at x = 0, 0.5 and 1.0.

Acknowledgements

This work was funded by the National Metal and Materials Technology Center, National Science and Technology Development Agency (NSTDA), Thailand, Grant No. MT-B-59-CER-07-313-I.

REFERENCES

1. Synnefa A., Santamouris M., Apostolakis K. (2007): On the development, optical properties and thermal performance of cool colored coatings for the urban environment. *Solar Energy*, *81*, 488-497. doi: 10.1016/j.solener.2006.08.005
2. Synnefa A., Santamouris M., Akbari H. (2007): Estimating the effect of using cool coatings on energy loads and thermal comfort in residential buildings in various climatic conditions. *Energy and Buildings*, *39*, 1167-1174. doi: 10.1016/j.enbuild.2007.01.004
3. Uemoto K. L., Sato N.M.N., John V.M. (2010): Estimating thermal performance of cool colored paints. *Energy and Buildings*, *42*, 17-22. doi: 10.1016/j.enbuild.2009.07.026
4. Jose S., Reddy M.L. (2013): Lanthanum-strontium copper silicates as intense blue inorganic pigments with high near-infrared reflectance. *Dyes and Pigments*, *98*, 540-546. doi: 10.1016/j.dyepig.2013.04.013
5. Zhang Y., Zhang Y., Zhao X., Zhang Y. (2016): Sol-gel synthesis and properties of europium-strontium copper silicates blue pigments with high near-infrared reflectance. *Dyes and Pigments*, *131*, 154-159. doi: 10.1016/j.dyepig.2016.04.011
6. Smith A.E., Comstock M.C., Subramanian M.A. (2016): Spectral properties of the UV absorbing and near-IR reflecting blue pigment, $YIn_{1-x}Mn_xO_3$. *Dyes and Pigments*, *133*, 214-221. doi: 10.1016/j.dyepig.2016.05.029
7. Thongkanluang T., Kittiauchawal T., Limsuwan P. (2011): Preparation and characterization of Cr_2O_3–TiO_2–Al_2O_3––V_2O_5 green pigment. *Ceramics International*, *37*, 543-548. doi: 10.1016/j.ceramint.2010.09.044
8. Jose S., Prakash A., Laha S., Natarajan S., Reddy M.L. (2014): Green colored nano-pigments derived from Y_2BaCuO_5: NIR reflective coatings. *Dyes and Pigments*, *107*, 118-126. doi: 10.1016/j.dyepig.2014.03.025
9. Zou J., Zheng W. (2016): TiO_2@$CoTiO_3$ complex green pigments with low cobalt content and tunable color properties. *Ceramics International*, *42*, 8198-8205. doi: 10.1016/j.ceramint.2016.02.029
10. Vishnu V.S., George G., Reddy M.L.P. (2010): Effect of molybdenum and praseodymium dopants on the optical properties of $Sm_2Ce_2O_7$: Tuning of band gaps to realize various color hues. *Dyes and Pigments*, *85*, 117-123. doi: 10.1016/j.dyepig.2009.10.012
11. Vishnu V.S., Reddy M. L. (2011): Near-infrared reflecting inorganic pigments based on molybdenum and praseodymium doped yttrium cerate: Synthesis, characterization and optical properties. *Solar Energy Materials and Solar Cells*, *95*, 2685-2692. doi: 10.1016/j.solmat.2011.05.042
12. George G., Vishnu V.S., Reddy M.L.P. (2011): The synthesis, characterization and optical properties of silicon and praseodymium doped Y_6MoO_{12} compounds: Environmentally benign inorganic pigments with high NIR reflectance. *Dyes and Pigments*, *88*, 109-115. doi: 10.1016/j.dyepig.2010.05.010
13. Wang J.L., Li Y.Q., Byon Y.J., Mei S.G., Zhang G.L. (2013): Synthesis and characterization of $NiTiO_3$ yellow nano pigment with high solar radiation reflection efficiency. *Powder Technology*, *235*, 303-306. doi:10.1016/j.powtec.2012.10.044
14. Schildhammer D., Fuhrmann G., Petschnig L., Weinberger N., Schottenberger H., Huppertz H. (2017): Synthesis and characterization of a new high NIR reflective ytterbium molybdenum oxide and related doped pigments. *Dyes and Pigments*, *138*, 90-99. doi: 10.1016/j.dyepig.2016.11.024
15. Thongkanluang T., Chirakanohaisarn N., Limsuwan P. (2012): Preparation of NIR reflective brown pigment. *Procedia Engineering*, *32*, 895-901. doi: 10.1016/j.proeng.2012.02.029
16. Liu L., Han A., Ye M., Feng W. (2015): The evaluation of thermal performance of cool coatings colored with high near-infrared reflective nano-brown inorganic pigments: Magnesium doped $ZnFe_2O_4$ compounds. *Solar Energy*, *113*, 48-56. doi: 10.1016/j.solener.2014.12.034
17. Sanada K., Morisawa Y., Ozaki Y. (2014): Environmentally friendly synthesis and physical and optical properties of highly reflective green-black pigments. *Journal of the Ceramic Society of Japan*, *122*, 322-328. doi: 10.2109/jcersj2.122.322
18. Oka R., Masui T. (2016): Synthesis and characterization of black pigments based on calcium manganese oxides for high near-infrared (NIR) reflectance. *RSC Advances*, *6*, 90952–90957. doi: 10.1039/c6ra21443f
19. Bao W., Ma F., Zhang Y., Hao X., Deng Z., Zou X., Gao W. (2016): Synthesis and characterization of Fe^{3+} doped $Co_{0.5}Mg_{0.5}Al_2O_4$ inorganic pigments with high near-infrared reflectance. *Powder Technology*, *292*, 7-13. doi: 10.1016/j.powtec.2016.01.013
20. López R., Gómez R. (2012): Band-gap energy estimation from diffuse reflectance measurements on sol-gel and commercial TiO_2: a comparative study. *Journal of Sol-Gel Science and Technology*, *61*, 1-7. doi: 10.1007/s10971-011-2582-9
21. Shannon R.D. (1976): Revised effective ionic radii and systematic studies of interatomic distances in halides and chalcogenides. *Acta Crystallographica*, A*32*, 751-767. doi: 10.1107/S0567739476001551
22. Pailhe N., Wattiaux A., Gaudon M., Demourgues A. (2008): Correlation between structural features and vis-NIR spectra of α-Fe_2O_3 hematite and AFe_2O_4 spinel oxides (A=Mg, Zn). *Journal of Solid State Chemistry*, *181*, 1040-1047. doi: 10.1016/j.jssc.2008.02.009
23. Suwan M., Sangwong N., Supothina S. (2017): Effect of Co and Pr doping on the properties of solar-reflective $ZnFe_2O_4$ dark pigment. *IOP Conference Series: Materials Science and Engineering*, *182*, 012003. doi: 10.1088/1757-899X/182/1/012003
24. Sui J., Zhang C., Li J., Cai W. (2012): Facile synthesis of multifunctional $ZnFe_2O_4$ nanoparticles in liquid polyols. *Journal of Nanoscience and Nanotechnology*, *12*, 3867-3872. doi: 10.1166/jnn.2012.5872
25. Hirthna, Sendhilnathan S., Rajan P.I., Adinaveen T. (2018): Synthesis and characterization of $NiFe_2O_4$ nanoparticles for the enhancement of direct sunlight photocatalytic degradation of methyl orange. *Journal of Superconductivity and Novel Magnetism*, *31*, 3315-3322. doi: 10.1007/s10948-018-4601-3
26. Manikandan A., Vijaya J.J., Sundararajan M., Meganathan C., Kennedy L.J., Bououdina M. (2013): Optical and

magnetic properties of Mg-doped $ZnFe_2O_4$ nanoparticles prepared by rapid microwave combustion method. *Superlattices and Microstructures*, *64*, 118-131. doi: 10.1016/j.spmi.2013.09.021

27. Tatarchuk T.R., Paliychuk N.D., Bououdina M., Al-Najar B., Pacia M., Macyk W., Shyichuk A. (2018): Effect of cobalt substitution on structural, elastic, magnetic and optical properties of zinc ferrite nanoparticles. *Journal of Alloys and Compounds*, *731*, 1256-1266. doi: 10.1016/j.jallcom.2017.10.103
28. Manikandan A., Kennedy L.J., Bououdina M., Vijaya J.J. (2014): Synthesis, optical and magnetic properties of pure and Co-doped $ZnFe_2O_4$ nanoparticles by microwave combustion method. *Journal of Magnetism and Magnetic Materials*, *349*, 249-258. doi: 10.1016/j.jmmm.2013.09.013
29. Kale R.B., Lokhande C.D. (2004): Influence of air annealing on the structural, optical and electrical properties of chemically deposited CdSe nano-crystallites. *Applied Surface Science*, *223*, 343-351. doi: 10.1016/j.apsusc.2003.09.022
30. Kislov N., Srinivasan S.S., Emirov Y., Stefanakos E.K. (2008): Optical absorption red and blue shifts in $ZnFe_2O_4$ nanoparticles. *Materials Science and Engineering: B153*, 70-77. doi: 10.1016/j.mseb.2008.10.032